ON THE GENERATION OF INFLOW TURBULENCE IN THE SIMULATIONS OF URBAN BOUNDARY LAYER

Hai-Feng Li

Department of Engineering Mechanics
Tsinghua University
Beijing 100084, PR China
tylihaifeng@163.com

Cui-Xiang Cui

Department of Engineering Mechanics
Tsinghua University
Beijing 100084, PR China
cgx@tsinghua.edu.cn

Wei-Xi Huang

Department of Engineering Mechanics
Tsinghua University
Beijing 100084, PR China
hwx@tsinghua.edu.cn

ABSTRACT

The development of turbulence in urban boundary layers is investigated by theoretical analysis. Results show that: 1) the error caused by Reynolds-stress amplitude decays downstream until the fully developed level is achieved; and 2) if the Reynolds stress is correct but the characteristic length scale of the inflow turbulence is larger/smaller than that of the fully developed level, turbulent kinetic energy (TKE) error increases immediately downstream of the inlet and then decreases further downstream. The changing rate of error of inflow turbulence in the streamwise direction weakens as the distance from the ground increases.

According to the results above, a new turbulence-generation method is proposed for the simulations of microscale flow and dispersion by coupling Large-eddy Simulation with mesoscale models. Validations is concentrated on the flow and near-field dispersion in an urban canopy. Results of the simulation over the Central Business District (CBD) of Oklahoma City (a point release of Intensive Observation Period 3 of Joint Urban 2003) demonstrate that the mean velocity, TKE, the scalar plume, and mean concentration are in fairly good agreement with the field measurements. This indicates that the coupling scheme with small-scale turbulence added by the present method is effective in calculating the complex flow and dispersion in urban canopies.

INTRODUCTION

Atmospheric boundary-layer flow is complex and of high Reynolds number, containing motions of vast scales. It is currently not feasible to simulate all the scales in a single model. Therefore, coupling methods were proposed to simulate finer flows of atmospheric environments, in which the boundary conditions of microscale models are provided by the mesoscale fields. However, the resolution of mesoscale models is far coarser than that of microscale models, e.g. Large Eddy Simulation (LES) in the present work. Therefore, the challenge is that the small-scale turbulence should be specified at the coupling interface.

In previous coupling simulations, buffer regions were used to generate small-scale turbulence (Liu et al. 2012, Nakayama et al. 2012, Michioka et al. 2013, Park et al. 2015). Liu et al. (2012) extended the LES domain for turbulence to develop naturally in the buffer region. Such method is simple, but with substantial increase in computational costs. Nakayama et al. (2012) and Park et al. (2015) rotated the x axis to the main wind direction and extracted fluctuations at the outflow plane of the buffer region by performing a lateral averaging to generate small-scale turbulence. However, the method has yet been validated in practical atmospheric simulations. Furthermore, two factors need to be met for this method: 1) the wind direction is steady and 2) the underlying surface is uniform in the lateral direction, which are rarely the case in actual urban areas.

To propose a new turbulence-generation method, two steps are taken. Firstly, the influence of inflow turbulence statistics on the downstream development of turbulence in urban boundary layer is investigated. Among all the turbulent statistics, the Reynolds stress and spectra of the inflow turbulent are concentrated in the present work. Secondly, a turbulence-generation method, which is used to provide small-scale turbulence at the coupling interface.

Under neutral stratification conditions, turbulence in the outer-layer (above the roughness sublayer, i.e. $z > 2.0h$) only depends on the friction velocity u_*, the height $z - d$ (with d being the zero-plane displacement height) and the boundary layer thickness δ, and this is summarized as the outer-layer similarity in Raupach et al. (1991). A databank of turbulence is set up for the outer-layer by a pre-computed turbulent flow, and then the turbulence is transformed to the coupling interface by outer-layer similarity. Within the inner-layer (below the roughness sublayer, i.e. $z > 2.0h$), on the other hand, turbulence is dynamically influenced by the underlying roughness. Therefore, turbulent flow in the inner-layer is case-dependent and databank for the inner-layer should be prepared according to the parameters of the target problem. The turbulence generated in the inner- and outer-layer are then combined by forming a weighted addition.

NUMERICAL METHOD

Microscale flow and dispersion in urban areas are considered, of which the governing equations are incompressible Navier-Stokes (N-S) equations with Boussinesq approximation. LES is applied in the present work. The filtered form of the continuity, the N-S equations and scalar equations are as follows:

$$\frac{\partial \hat{u}_i}{\partial x_i} = 0 \tag{1}$$

$$\frac{\partial \hat{u}_i}{\partial t} + \hat{u}_j \frac{\partial \hat{u}_i}{\partial x_j} = -\frac{1}{\rho}\frac{\partial \hat{p}}{\partial x_i} + \nu \frac{\partial^2 \hat{u}_i}{\partial x_j \partial x_j} + \frac{\partial \tau_{ij}}{\partial x_j} + \frac{\hat{\theta} - \hat{\theta}_0}{\hat{\theta}_0} g\delta_{i3} + \hat{f}_i \tag{2}$$

$$\frac{\partial \hat{\theta}}{\partial t} + \hat{u}_j \frac{\partial \hat{\theta}}{\partial x_j} = \kappa \frac{\partial^2 \hat{\theta}}{\partial x_j \partial x_j} + \frac{\partial \tau_{\theta j}}{\partial x_j} + \hat{S}_\theta \tag{3}$$

$$\frac{\partial \hat{c}}{\partial t} + \hat{u}_j \frac{\partial \hat{c}}{\partial x_j} = D \frac{\partial^2 \hat{c}}{\partial x_j \partial x_j} + \frac{\partial \tau_{cj}}{\partial x_j} + \hat{S}_c \tag{4}$$

Here, three coordinates are denoted as x, y, z (or x_1, x_2, x_3). $\hat{u}, \hat{v}, \hat{w}$ (or $\hat{u}_1, \hat{u}_2, \hat{u}_3$) are the filtered velocity of the longitudinal, latitudinal and vertical direction. $\hat{\theta}$, $\hat{p}$ and $\hat{c}$ are the filtered temperature, pressure and scalar concentration. Reference temperature, air density and the kinematic viscosity coefficient are $\hat{\theta}_0 = 303.15K$, $\rho = 1.208\,\mathrm{kg\,m^{-3}}$ and $\nu = 1.5\times10^{-5}\,\mathrm{m^2\,s^{-2}}$. The thermal diffusivity and the mass diffusivity are $\kappa = \nu/\mathrm{Pr}$ and $D = \nu/\mathrm{Sc}$. The Prandtl number Pr and Schmidt number Sc are both set to be 0.72. The symbols $\hat{f}_i$, $\hat{S}_\theta$ and $\hat{S}_c$ are external body force, the heat source and the scalar release rate, respectively.

$\tau_{ij} = \widehat{u_i u_j} - \hat{u}_i \hat{u}_j$, $\tau_{\theta j} = \widehat{\theta u_j} - \hat{\theta}\hat{u}_j$ and $\tau_{cj} = \widehat{c u_j} - \hat{c}\hat{u}_j$ are the sub-grid stress, sub-grid thermal flux and sub-grid mass flux respectively, which are closed by Smagoringsky model.

The equations are discretized with finite volume method on non-staggered grids. A third order explicit Runge-Kutta scheme is applied in time integration. Wall models of velocity for the wind field (Grötzbach 1987) and temperature for the thermal field (Defraeye et al. 2011) are adopted.

DEVELOPMENT OF INFLOW TURBULENCE

In this section, we investigate the development of inflow turbulence in urban boundary-layer. A turbulenet flow field with homogeneous mean velocity field is assumed:

$$U(z), V = W = 0 \tag{5}$$

where U, V, W are averaged in time and in the lateral direction, and Eq. 5 is valid for $z > 1.5h$. With a fully-developed turbulent field at the inflow boundary, the turbulent statistics are also homogenerous in the streamwise direction. In this condition, the characteristic turbulent velocity, characteristic length scale, Reynolds stress and turbulent kinetic energy (TKE) are denoted as u^0, $l^0(z)$, $R_{ij}^0(z)$ and $\mathcal{K}^0 = R_{ii}^0/2$ respectively.

If turbulent field is not fully developed at the inlet, it will experience an adjustment in the streamwise direction. In this case, the perturbation of mean velocity is negligible and thus Eq. 5 is still valid. The characteristic turbulent velocity, characteristic length scale, and Reynolds stress are denoted as $u^e = E(x,z)u^0$, $l^e(x,z)$, $R_{ij}^e(x,z) = E^2 R_{ij}^0(z)$, and TKE is $\mathcal{K}^e = R_{ii}^e/2 = E^2\mathcal{K}^0$.

By neglecting the dispersion term in TKE budget equations, the development of $E(x,z)$ can be obtained:

$$\frac{\partial E}{\partial x} = -\frac{\lambda^0}{2U(z)}\frac{\partial U(z)}{\partial z}\left(-E + E^2\frac{l^0}{l^e}\right) \tag{6}$$

λ^0 is defined by $-\langle u'w'\rangle^0 = \lambda^0 \mathcal{K}^0$. Note that, in derivation of the governing equation of E, the influence of spectra is simplified as the characteristics length scale.

For $l^0/l^e = 1$, integrating Eq. 6 from 0 to x gives:

$$E = \frac{1}{\left(1-(1-1/E_1)\exp\left(-x/D(z)\right)\right)} \tag{7}$$

where, $D(z) = 2U(z)\Big/\left(\lambda^0 \partial U(z)/\partial z\right)$ and is the length scale that characterizes decaying rate of the inlet flow error. In boundary-layer flows, $\lambda^0 > 0$ and is constant for most part of the boundary depth. Therefore, $D(z)$ increases with the distance from the ground. It is apparent that $E|_{x=\infty} = 1.0$ and it can be concluded that: the error caused by Reynolds stress amplitude decays downstream until the fully developed level is achieved.

For $E_1 = 1$, that the amplitude of the TKE is the same as that of the fully developed turbulence while the characteristic length scale of the inlet turbulence l_1^e is different from that of the fully developed level l^0, l^e adjusts to l^0 downstream because of the rebuild of turbulent cascade process. For simplicity, the short distance downstream is considered so that the change of l^e is negligible and thus $l^e \approx l_1^e(z)$. Then integrating Eq. 6 gives:

$$E = \frac{1}{\frac{l^0}{l^e}\left(1-\left(1-\frac{l^e}{l^0}\right)\exp\left(-x/D(z)\right)\right)} \tag{8}$$

Similarly, $D(z)$ is the length scale that characterizes changing rate of the flow field. Thus, the changing rate weakens as z increases. Some qualitative conclusions can be made in the region immediately downstream of the inlet as follows:

1) If the inflow integral length scale is larger than that of the fully developed level, i.e. $l^e/l^0 > 1$, then TKE and E will increase as x increases.

2) If the inflow characteristic length scale is smaller than that of the fully developed level, i.e. $l^e/l^0 < 1$, then TKE and E will decrease as x increases.

The length scale $D(z)$ is partly determined by the convection velocity $U(z)$, which carries the inlet data error downstream, and partly by the gradient of the mean velocity $\partial U(z)/\partial z$, which determines the level of shear production. Thus, for flows in which high shear regions are prominent, the distance needed for the turbulence to develop fully is quite short.

TURBULENCE GENERATION METHOD

It can be concluded from the results in the previous section that both the Reynolds stress, which determines the amplitude of the fluctuations, and the spectra, which determines the length scale and structures of the fluctuations, are important for the development of inflow turbulence. Accordingly, a new turbulence-generation method is proposed in the present section.

The idea of generating turbulence at the coupling interface has been introduced in Sect. Introduction. The parameters needed are listed in Table. 1 and the detailed steps are as follows:

Step 1. Prepare a databank for the outer-layer, denoted as $(u_i)_{outer}=(U_i)_{outer}+(u_i')_{outer}$, where $(U_i)_{outer}$ is the mean velocity, and $(u_i')_{outer}$ is the fluctuation field. The databank can be a flow over a cluster of model buildings, driven by a pressure gradient, with periodic conditions in the horizontal direction. The boundary layer thickness, zero-plane displacement height, and friction velocity of the databank are $(\delta)_{outer}$, $(d)_{outer}$, and $(u_*)_{outer}$, respectively. The fluctuation field $(u_i')_{outer}$ is scaled according to the outer-layer similarity as follows:

$$\frac{(u_i')^{outer}_{target}((\bar{x}_i)_{target},(\bar{t})_{target})}{(u_*)_{target}}=\frac{(u_i')_{outer}((\bar{x}_i)_{outer},(\bar{t})_{outer})}{(u_*)_{outer}} \tag{9.a}$$

$$(\bar{x}_i)_{target}=\begin{cases}\dfrac{(x_i)_{target}}{(\delta)_{target}} & i=1,2\\ \dfrac{(x_i)_{target}-(d)_{target}}{(\delta)_{target}-(d)_{target}} & i=3\end{cases}. \tag{9.b}$$

$$(\bar{t})_{target}=\frac{t_{target}}{(\delta)_{target}/(u_*)_{target}} \tag{9.c}$$

$$(\bar{x}_i)_{outer}=\begin{cases}\dfrac{(x_i)_{outer}}{(\delta)_{outer}} & i=1,2\\ \dfrac{(x_i)_{outer}-(d)_{outer}}{(\delta)_{outer}-(d)_{outer}} & i=3\end{cases}. \tag{9.d}$$

$$(\bar{t})_{outer}=\frac{t_{outer}}{(\delta)_{outer}/(u_*)_{outer}} \tag{9.e}$$

where $(u_i')^{outer}_{target}$ is the target fluctuation field in the outer-layer. $(\bar{x}_i)_{target}$ and $(\bar{t})_{target}$, defined as Eq. (9.b), (9.c), are scaled coordinates and time of the target problems. $(\bar{x}_i)_{outer}$ and $(\bar{t})_{outer}$, defined as Eq. (9.d), (9.e), are scaled coordinates and time of the outer-layer databank.

Step 2. To prepare a databank for the inner-layer, a cluster of model-building arrays should be constructed. The geometrical parameters of the model building arrays, i.e. mean height, projection area ratio and frontal area ratio of the arrays, should be consistent with that of the target problem. After that, the mesoscale velocity is used to drive the flow over the model building arrays. The databank is $(u_i)_{inner}=(U_i)_{inner}+(u_i')_{inner}$, where $(U_i)_{inner}$ is the mean velocity and $(u_i')_{inner}$ is the fluctuation field. The turbulent field $(u_i')_{inner}$ is interpolated onto the target grid as:

$$(u_i')^{inner}_{target}((x_i)_{target},t_{target})=(u_i')_{inner}((x_i)_{inner},t_{inner}) \tag{10}$$

Step 3. The composite turbulent field at the coupling interface is:

$$(u_i')_{target}=(u_i')^{outer}_{target}W(\eta)+(u_i')^{innner}_{target}(1-W(\eta)) \tag{11}$$

where $W(\eta)$ is the weighting function:

$$W(\eta)=\frac{1}{2}\left\{1+\tanh\left[\frac{\alpha(\eta-b)}{(1-2b)\eta+b}\right]\Big/\tanh(\alpha)\right\} \tag{12}$$

In Eq. (12), $\eta=z/\delta_{tg}$, and b is the transition height between outer-layer and inner-layer. $\alpha=10$, determining the transition width. As a result, the weighting function is 0 at $\eta=0$, 0.5 at $\eta=b$, and 1 at $\eta=1$.

Table 1. Input parameters of the target problems that are needed for the turbulence generation.

Parameter	Definition	Source
$(h)_{target}$	Mean height of buildings	1
$(d)_{target}$	Zero-plane displacement height	1
$(\lambda_p)_{target}$	Projection area ratio	1
$(\lambda_f)_{target}$	Frontal area ratio	1
$(\delta)_{target}$	Boundary layer depth	2
$(u_*)_{target}$	Friction velocity	2

Notes: 1: Geometrical data; 2: Mesoscale models.

FLOW AND DISPERSION OVER AN ACTUAL URBAN AREA

In this section, a microscale atmospheric flow with scalar dispersion over the Central Business District (CBD) of Oklahoma City (OKC) (a point release of Intensive Observation Period 3 of Joint Urban 2003) is simulated with the coupling method. The small-scale turbulence is added at the coupling interface and the results are compared with the field observations.

Numerical Configurations

The mesoscale flow is provided by the Advanced Research WRF model (ARW) version 3.8.1. Fig. 1(a) shows the 5 nested domains of WRF. The horizontal grid spacing (number of grid nodes) of each domain are 40.5 km (103×103), 13.5 km (103×103), 4.5 km (103×103), 1.5 km (103×103), and 0.5 km (145×145 . There are 50 vertical levels, with 17 layers below the first 1000 metres above the ground. The pressure at the top of the domain is 50 hPa. A 24-hours WRF simulation beginning at 0000UTC July 7, 2003 and ending at 0000UTC July 8, 2003, is conducted, of which the initial and boundary data are from the National Centre for Environmental Prediction (NCEP) operational Global Final (FNL) Analyses on a 1.0×1.0 -degree resolution. The Yonsei University (YSU) (Hong et al. 2006) planetary boundary-layer scheme is employed. The Rapid Radiative Transfer Model (RRTM) (Mlawer et al. 1997) is used for long wave radiation, and Dudhia (Wei et al. 2016) is applied as shortwave radiation model. Noah Land-Surface Model is used for the land-surface option. The CBD of OKC is located in the centre of the WRF domains and the results of the innermost domain are saved every 15 minutes to provide initial and boundary conditions for the LES model.

Figure 1(b) is the sketch of the horizontal LES domain. The size of the LES domain $L_x\times L_y\times L_z$ is $1728\times1728\times471$m . The simulation begins at 1545UTC and ends at 1645UTC. Scalar is released 15 minutes after the initiation for half hour.

On the ground, the temperature is determined by a thermal balance model (Noilhan and Planton 1989), accounting for radiation, sensible heat fluxes, latent heat fluxes and the heat conduction into the deep ground. On the surface of the buildings, the same thermal balance model is applied, taking the shadowing effect of the solar radiation into account, while the thermal conduction into the buildings is omitted (Liu et al. 2012).

On the western, southern and top boundary of the domain, the wind field and temperature of WRF results are interpolated onto the LES grid. Above the first grid point of WRF, trilinear interpolation is applied. Below the first grid point of WRF, interpolation is conducted assuming a power law of wind field and temperature near the ground (Liu et al. 2012). The turbulence generation method is used to add small-scale turbulence at the coupling interface. On the eastern and northern boundary of the domain, where the flow is outward, a non-reflecting condition is used.

For the scalar field, zero mass-flux boundary condition is applied on the solid surfaces as well as at the western and southern boundary. At the northern, eastern and top boundary, a non-reflecting condition is used.

The point source (red balloon) is located at the north-east corner of the Botanical Garden (the orange rectangle). The height of the point source is 1.9 m above the ground. The blue rectangle area represents the region of interest, of which the size is designed so as to capture the near-field dispersion. In the region of interest, the buildings are resolved with a fine grid resolution.

The trees in the Botanical Garden are represented by drag elements. The drag force is added in the momentum equations. The empirical formula of Lalic and Mihailovic (2004) is applied to obtained the leaf-area density.

Outside the blue rectangle area, a buffer region is arranged, where the grid is coarse and the buildings are treated as drag elements (Liu et al. 2012).

In the region of interest, the horizontal grid spacing is 1 m or 3 m. The grids are stretched in the buffer region, with the largest grid spacing being 27 m. In the vertical direction, the grids are uniform below z = 20 m and above z = 130 m, with the grid spacing being 1 m and 18 m, respectively. In the interval between z = 20 m and z = 130 m, the grid spacing is stretched from 1 m to 18 m with a ratio of 1.2. The total grid number is $348\times382\times56$. The time step of LES model in the present work is 0.02 seconds.

The case with small-scale turbulence added at the coupling interface (i.e. the present new coupling scheme) is denoted as New-CP. Case Pre-CP is performed without adding small-scale turbulence at the coupling interface (i.e. the previous coupling scheme) for comparison.

Results and Discussion

The results of the present work and the observations are given. Without otherwise indication, the results are 30-minutes averaged.

To evaluate the performance of the models, five metrics (Hanna et al. 2004) are used for the prediction of flow and scalar. The metrics include: the fractional bias (FB), the geometric mean bias (MG), the normalized mean square error (NMSE), the geometric variance (VG), and the fraction of predictions within a factor of 2 of observations (FAC2).

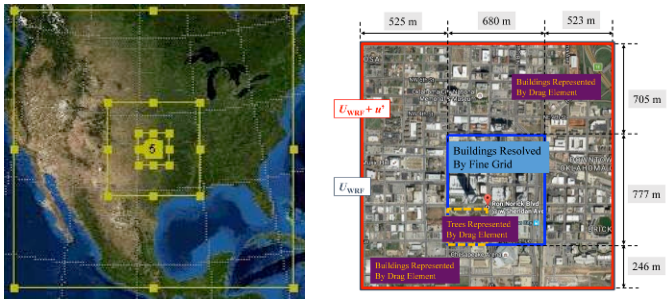

(a) (b)

Figure 1 Computational domains of (a) WRF model and (b) LES model.

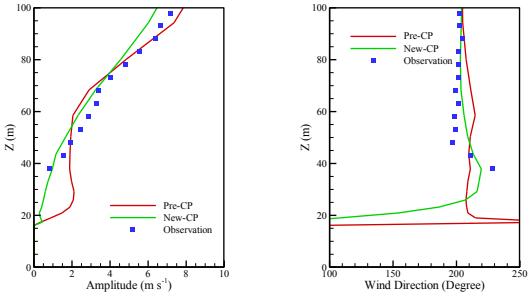

(a) (b)

Figure 2. Vertical profiles of mean velocity at x = 1026 m, y = 933 m. (a) Wind amplitude and (b) wind direction.

Wind Field.

The vertical profiles of mean wind speed and wind direction are shown in Fig. 2. The sampling point is located in the central region, above an 18-metres high building. The agreement between the predictions and observations is satisfactory, indicating that the influence of underlying surface on the flow field is well captured. The results of New-CP are better than that of Pre-CP, demonstrating the effectiveness of the turbulence added at the coupling interface.

Table 2 Evaluation statistics for TKE at sampling locations.

Case	FB(0)	MG(1)	NMSE(0)	VG(1)	FAC2(1)
Pre-CP	0.383	1.72	0.400	2.46	0.750
New-CP	-0.098	0.90	0.108	1.16	0.950

Table 3 Evaluation statistics for scalar at sampling locations.

Case	FB(0)	MG(1)	NMSE(0)	VG(1)	FAC2(1)
Pre-CP	0.302	3.30	2.62	1317	0.421
New-CP	0.855	1.00	9.56	6.04	0.579

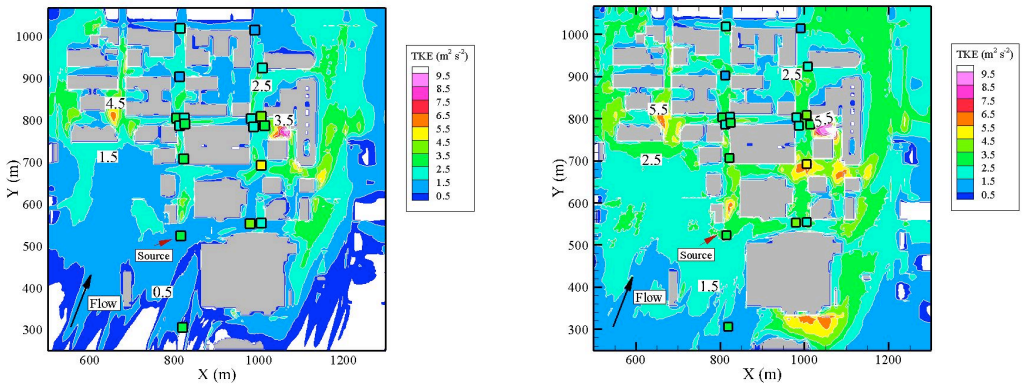

(a) (b)

Figure 3 Contours of TKE of an *x*-*y* slice at z = 8 m. (a) Pre-CP; (b) New-CP. Observations are denoted as squares.

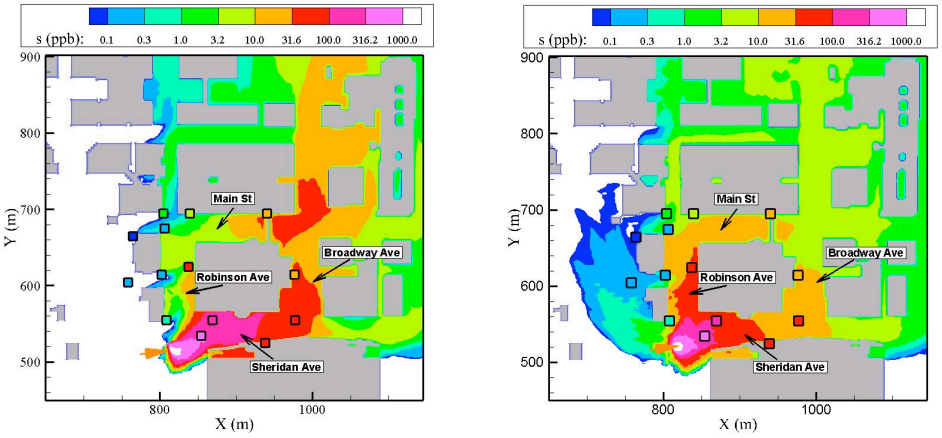

(a) (b)

Figure 4 Scalar concentration at street level (z = 1 m) of (a) Pre-CP and (b) New-CP. Observations are denoted as squares.

Coceal et al. (2006) suggested that the unsteady effects in the lower canopy are important because turbulent fluctuations dominate over the mean flow. Therefore, the accuracy of TKE in the canopy layer, especially near the source location is crucial for near-field dispersions. TKE of the numerical results are shown in Fig. 3. In Fig. 3, the slice height z = 8 m is less than half of the average building height and the TKE of observations are shown by the squares for comparison. In Fig. 3(a), TKE is kept at low level until it flows through the central region, where the wind shear and wake effects accelerate the turbulent production. The comparison shows that TKE is underestimated in the region of y < 700 m for Pre-CP. While for New-CP, the calculated TKE agrees well with the observations, especially at the source location (indicated by the orange arrow). Evaluation statistics for TKE results are listed in Table 2 (Values in the brackets are for a perfect model), further demonstrating that the results are

improved in TKE predictions with the small-scale turbulence added in the coupling method.

Scalar field.

In Fig. 4, 15-minutes averaged near-field scalar plume at the street level is shown. For Pre-CP, scalar is mainly transported downstream along Sheridan Avenue and then Broadway Avenue, where scalar concentration is high. At the intersection between Broadway Avenue and Main Street, a local high concentration appears because of the positive scalar flux from Main Street. By contrast, the concentration along and to the west of Robinson Avenue is smaller than the observations. For New-CP, high concentration appears immediately downstream of the source in both Sheridan Avenue and Robison Avenue. Thus the observed split-plume (as the squares indicate) are well predicted. Scalar concentration to the west of Robison Ave agrees quite well with the observations. The plume of New-CP is wider than that of Pre-CP, clearly caused by the enhanced turbulent field. This effect of turbulence on the plume is consistent with previous researches (Chan and Leach 2004). As it flows downstream, the concentration along Main Street is correspondingly higher and concentration along the northern Broadway Avenue is lower than that of Pre-CP.

The evaluation statistics for the near-field dispersion are listed in Table 3. Overall, the results are improved with the small-scale turbulence added at the coupling interface. The exceptions are FB and NMSE, which are sensitive to observed and/or predicted values that may be particularly high. By contrast, the logarithmic measures of MG and VG can provide a more balanced treatment of extreme high values. With the current case, Pre-CP and Ref overestimate the near-field concentration and thus generate smaller FB and NMSE.

CONCLUSION

The development of inlet turbulence in MUAE flows is investigated by neglecting the dispersion terms in TKE budget equations. It is concluded that: 1) the error caused by Reynolds-stress amplitude decays downstream until the fully developed level is achieved; and 2) if the Reynolds stress is correct but the characteristic length scale of the inflow turbulence is larger or smaller than that of the fully developed level, TKE error increases immediately downstream of the inlet and then decreases further downstream. A length scale, $D(z)$, is deduced, which indicates that the changing rate of error of inlet data in the streamwise direction weakens as the distance from the ground increases.

Accordingly, a new turbulence-generation method is proposed for the simulations of microscale flow and dispersion by coupling LES with mesoscale models. The method is validated in the simulation of microscale flow with dispersion over CBD, a densely-built urban area in OKC. With proper small-scale turbulence added at the coupling interface, the predictions of mean field in the central region, TKE in the canopy layer are improved. The scalar plume and the mean concentration are in good agreement with the observations with small-scale turbulence added at the coupling interface. This indicates that the coupling scheme with small-scale turbulence added by the present turbulence-generation method is effective in calculating the complex flow and dispersion in urban canopies.

REFERENCES

Chan, S. T. and M. J. Leach (2004), "Large Eddy Simulation of an URBAN 2000 Experiment with Various Time Dependent Forcing". *the Fifth Symposium on the Urban Environment*, Vancouver, British Columbia, Canada.

Coceal, O., et al. (2006), "Mean Flow and Turbulence Statistics Over Groups of Urban-like Cubical Obstacles." *Boundary-Layer Meteorology* Vol. **121**: pp. 491-519.

Defraeye, T., et al. (2011), "An Adjusted Temperature Wall Function for Turbulent Forced Convective Heat Transfer for Bluff Bodies in the Atmospheric Boundary Layer." *Building and Environment* Vol. **46**: pp. 2130-2141.

Grötzbach, G. (1987), "Direct Numerical and Large Eddy Simulation of Turbulent Channel Flows." *Encyclopedia of fluid mechanics* Vol. **6**: pp. 1337-1391.

Hanna, S. R., et al. (2004), "FLACS CFD Air Quality Model Performance Evaluation with Kit Fox, MUST, Prairie Grass, and EMU Observations." *Atmospheric Environment* Vol. **38**: pp. 4675-4687.

Hong, S. Y., et al. (2006), "A New Vertical Diffusion Package with an Xxplicit Treatment of Entrainment processes." *Monthly Weather Review* Vol. **134**: pp. 2318-2341.

Lalic, B. and D. T. Mihailovic (2004), " An Empirical Relation Describing Leaf-area Density Inside the Forest for Environmental Modeling." *Journal of Applied Meteorology* Vol. **43**: pp. 641-645.

Liu, Y. S., et al. (2012), "Study on Micro-atmospheric Environment by Coupling Large Eddy Simulation with Mesoscale Model." *Journal of Wind Engineering and Industrial Aerodynamics* Vol. **107-108**: pp. 106-117.

Michioka, T., et al. (2013), "Large-eddy Simulation Coupled to Mesoscale Meteorological Model for Gas Dispersion in an Urban District." *Atmospheric Environment* Vol. **75**: pp. 153-162.

Mlawer, E. J., et al. (1997), "Radiative Transfer for Inhomogeneous Atmospheres: RRTM, a Validated Correlated-k Model for the Longwave." *Journal of Geophysical Research: Atmospheres* Vol. **102**: pp. 16663-16682.

Nakayama, H., et al. (2012), "Large-eddy Simulation of Urban Boundary-layer Flows by Generating Turbulent Inflows From Mesoscale Meteorological Simulations." *Atmospheric Science Letters* Vol. **13**: pp. 180-186.

Noilhan, J. and S. Planton (1989), "A Simple Parameterization of Land Surface Processes for Meteorological Models. ." *Monthly Weather Review* Vol. **117**: pp. 536-549.

Park, S.-B., et al. (2015), "Impacts of Mesoscale Wind on Turbulent Flow and Ventilation in a Densely Built-up Urban Area." *Journal of Applied Meteorology and Climatology* Vol. **54**: pp. 811-824.

Raupach, M. R., et al. (1991), " Rough-Wall Turbulent Boundary Layers." *Appl. Mech. Rev* Vol. **44**: pp. 1-25.

Wei, X., et al. (2016), "Experimental and Numerical Study of Wind and Turbulence in a Near-Field Dispersion Campaign at an Inhomogeneous Site." *Boundary-Layer Meteorology* Vol. **160**: pp. 475-499.